Supplementary material

"Emotion self-regulation training in major depressive disorder using simultaneous real-time fMRI and EEG neurofeedback" by V. Zotev et al.

S1.1. Modified MR-compatible EEG cap

To achieve more efficient real-time EEG-fMRI artifact suppression, we modified a 32-channel BrainCap-MR (EASYCAP, GmbH) as shown in Fig. 2D. In the modified cap, four EEG channels out of 31 – FC1, FC2, TP9, TP10 – were re-purposed for acquisition of reference artifact waveforms, which we refer to as $R_1(t)$, $R_2(t)$, $R_3(t)$, and $R_4(t)$, instead of EEG activity. For each of these channels, the lead was disconnected from its electrode, and connected to one end of a wire contour. The other end of the contour was connected to the Ref electrode (FCz, blue) via a 50 kOhm resistor. Geometries of the four contours were optimized so that electromotive forces (EMFs), induced in the contours during head movements in the MRI scanner's main field, approximate cardioballistic (CB) and random-motion artifacts picked up by EEG channels F3 and F4. The two shorter contours (brown wires in Fig. 2D) followed the leads of channels F3 and F4, respectively, then looped around the Gnd electrode (AFz, black), and connected to the Ref via the resistors. The two longer contours (orange wires in Fig. 2D) also followed the leads of F3 and F4, looped around electrodes Fp1 and Fp2, respectively, then around the Gnd, and connected to the Ref through the resistors. The resistors were non-magnetic non-inductive surface mount thin film resistors (Vishay PNM1206-50KBCT-ND, 50k, 0.1%, 0.4W). After the cap had been placed and aligned on a participant's head, the wire contours were fixed tightly to the cap's fabric with adhesive tape (3M Durapore). This EEG cap modification enabled acquisition of the four reference artifact waveforms, along with 27 EEG waveforms and one ECG waveform, using the standard 32-channel system configuration. Importantly, the use of the modified EEG cap did not affect quality of structural or functional MRI brain images.

S1.2. Performance of the real-time EEG artifact regression

Figure S1 evaluates effectiveness of the real-time regression of the CB and motion artifacts (Sec. 2.5, Fig. 3) with the linear regression coefficients $\{a_i\}$, $\{b_i\}$, i=1…4, based on the previous run as opposed to the current run. The actual real-time signal variance changes for channels F3 and F4 (same as in Fig. 3C) after the regression procedure with the coefficients for a current run determined by fitting the data for the previous run are shown along the y-axis in Fig. S1. The corresponding variance changes after an offline regression procedure with the optimum regression coefficients for a current run are shown along the x-axis. The results are pooled across five task runs for all participants. The plots in Fig. S1 demonstrate high correlation (r=0.98) between the two quantities. A few outlier points (included in the statistics computation) out of total n=120 points in each plot correspond to situations when a current run is characterized by a very drastic (usually one per run) head motion, not present during the previous run, or vice versa. The linear fits to the data for F3 and F4 have slopes of 0.96 and 0.98, respectively (Fig. S1). Therefore, the use of the regression coefficients optimized for the previous run yields signal variance reduction that is 96-98%, on the average, of the variance reduction achieved with the regression coefficients optimized for the current run. These results justify our proposed implementation of the linear regression procedure for improved real-time EEG-fMRI artifact correction, described in Sec. 2.5.

S1.3. Reliability of the real-time EEG artifact correction

Figure S2 compares the EEG-nf target measures computed in real time and the corresponding measures determined in offline EEG data analysis. The relative frontal EEG asymmetries A and B were computed every 2 s (Sec. 2.6) following the real-time EEG-fMRI artifact correction procedure (Sec. 2.5), and their values were saved to a file during each run. The real-time A and B data, reported in Fig. S2, were taken from these files. The offline EEG data processing was applied to the raw EEG data recorded during fMRI. It included average artifact subtraction (AAS) for MR artifacts, followed by AAS for CB artifacts, and exclusion of bad intervals, as described in detail below (S1.6). The offline A and B data in Fig. S2 were computed after such processing.

Mean real-time A values for the Happy Memories conditions in each run and the corresponding mean offline A values are compared in Fig. S2A. The results are pooled across five task runs for all participants. Fig. S2B compares mean real-time A changes and mean offline A changes between the Rest and Happy Memories conditions. Similar plots for the B values and B changes are shown in Figs. S2C and S2D. The correlations in Figs. S2A-D are highly significant with large effect sizes ($r>0.5$). These results suggest that the real-time EEG-nf target measures were sufficiently reliable, both for the alpha band (A) and for the high-beta band (B). The differences between the real-time and offline data in Fig. S2 can be attributed to the following factors. First, the offline AAS procedures for MR and CB artifacts are more accurate than the corresponding real-time AAS procedures, because they involve careful visual inspection of the artifact patterns across an entire run and manual adjustment of the correction parameters (semi-automatic correction mode). Second, the real-time artifact regression procedure (Fig. 3B) can reduce some CB artifacts that cannot be efficiently suppressed by the offline AAS, e.g. due to large variations in CB artifacts' temporal profiles.

S1.4. fMRI data analysis

Offline analysis of the fMRI data was performed in AFNI (Cox, 1996; Cox and Hyde, 1997). Pre-processing of single-subject fMRI data included time series despiking using the 3dDespike AFNI program with -localedit option. It was followed by correction of cardiorespiratory artifacts using the AFNI implementation of the RETROICOR method (Glover et al., 2000). Further fMRI pre-processing involved slice timing correction and volume registration of all EPI volumes acquired in the experiment using the 3dvolreg AFNI program with two-pass registration. The last volume of the short EPI dataset, acquired immediately after the high-resolution anatomical MPRAGE brain image (Sec. 2.6), was used as the registration base.

To enable transformation of the fMRI data to the Talairach space, the Talairach transform was first performed for each subject's high-resolution anatomical MPRAGE brain image. The image was subjected to explicit skull-stripping using the 3dSkullStrip AFNI program with -blur_fwhm option, and then transformed towards the standard TT_N27 template in the Talairach space using the @auto_tlrc AFNI program.

The fMRI activation analysis was performed according to the standard general linear model (GLM) approach. It was conducted for each of the five task fMRI runs (Fig. 1B) using the 3dDeconvolve AFNI program. The GLM model included two block-design stimulus condition terms, Happy Memories and Count, represented by the standard block-stimulus regressors in AFNI. A general linear test (-gltsym) term was included to compute the Happy vs Count contrast. Nuisance covariates included the six fMRI motion parameters and five polynomial terms for modeling the baseline. To further reduce effects of residual motion artifacts, the fMRI data and motion parameters were lowpass Fourier filtered at 0.1 Hz prior to the GLM analysis. GLM β coefficients were computed for each voxel, and average percent signal changes for Happy vs Rest, Count vs Rest, and Happy vs Count contrasts were obtained by dividing the corresponding β values (×100%) by the β value for the constant baseline term. The resulting fMRI percent signal change maps for each run were transformed to the Talairach space by means of the @auto_tlrc AFNI program. The individual high-resolution anatomical brain image in the Talairach space was used as the transformation template. The maps were re-sampled to $2\times2\times2$ mm^3 isotropic voxel size.

Average individual BOLD activity levels were computed in the offline analysis for the LA and L rACC target ROIs, exhibited in Figs. 2A,B. The voxel-wise fMRI percent signal change data from the GLM analysis, transformed to the Talairach space, were averaged within these ROIs and used as GLM-based measures of these regions' BOLD activities.

To compare BOLD activity levels for the left and right amygdala, we considered amygdala BOLD laterality, i.e. a difference in mean GLM-based fMRI percent signal changes between the LA and RA ROIs for each contrast, run, and participant. The LA and RA ROIs in this case were defined as the left and right amygdala regions specified in the AFNI implementation of the Talairach-Tournoux brain atlas. Similarly, we computed BOLD laterality for the middle frontal gyrus (MidFG) as a difference in mean GLM-based fMRI percent signal changes between the left and right MidFG ROIs. The ROIs were defined as the left and right middle frontal gyrus regions specified in the AFNI implementation of the Talairach-Tournoux atlas, and limited to a selected slab along z-axis ($z_1 \leq z \leq z_2$).

S1.5. fMRI-based PPI analysis

To evaluate changes in the left amygdala fMRI functional connectivity between experimental conditions, we conducted a psychophysiological interaction (PPI) analysis (Friston et al., 1997; Gitelman et al., 2003). The analysis was based on fMRI time course for an LA seed ROI. The seed ROI was defined as the left amygdala region specified in the AFNI implementation of the Talairach-Tournoux brain atlas. (We used the anatomical amygdala ROI, because the spherical LA target ROI (Fig. 2A) includes some voxels outside the amygdala proper). The seed ROI was transformed to each subject's individual EPI space. In addition, 10-mm-diameter ROIs were defined within the left and right frontal white matter (WM) and within the left and right ventricle cerebrospinal fluid (CSF) using the individual high-resolution anatomical brain image in the Talairach space

(S1.4), and also transformed to the EPI space. The pre-processed fMRI data and the six fMRI motion parameters were bandpass filtered between 0.01 and 0.08 Hz using the 3dTproject AFNI program. The 3dmaskave AFNI program was then used to compute average fMRI time courses for the LA, WM, and CSF ROIs. The LA seed ROI time course was employed as the fMRI-based PPI correlation regressor. A PPI interaction regressor was defined for the Happy Memories vs Rest condition contrast as follows. A [Happy−Rest] contrast function was defined to be equal +1 for the Happy Memories condition blocks, −1 for the preceding Rest condition blocks, and 0 for all other condition blocks (Fig. 1B). The LA time course was detrended, using the 3dTproject AFNI program, with respect to the time courses of the six fMRI motion parameters (together with the same time courses shifted by one *TR*), the time courses for the WM and CSF ROIs, and five polynomial terms. It was then deconvolved using the 3dTfitter AFNI program to estimate a time course of the underlying neuronal activity. This estimated 'neuronal' time course was multiplied by the [Happy−Rest] contrast function, and convolved with the same hemodynamic response function (HRF, 'Cox special') using the waver AFNI program. The resulting waveform was employed as the fMRI-based PPI interaction regressor for the Happy Memories vs Rest condition contrast.

A single-subject fMRI-based PPI analysis involved fitting a GLM model with the two PPI regressors using the 3dDeconvolve AFNI program. The GLM design matrix for each task run included four stimulus regressors, sixteen covariates of no interest, and five polynomial terms for modeling the baseline. The stimulus regressors included the fMRI-based PPI interaction regressor, the fMRI-based PPI correlation regressor, the Happy Memories block-stimulus regressor, and the Count block-stimulus regressor. The last two regressors were the standard block-design fMRI regressors in AFNI corresponding to the stimulus waveforms with 40-s-long condition blocks (Fig. 1B). The covariates of no interest included time courses of the six fMRI motion parameters, time courses of the same parameters shifted by one *TR*, time courses of the left and right WM ROIs, and time courses of the left and right ventricle CSF ROIs. Each single-subject PPI analysis produced GLM-based R^2-statistics and *t*-statistics maps for the fMRI-based PPI interaction and correlation terms for each run. These statistics were used to compute voxel-wise PPI interaction and correlation values. The resulting maps were subjected to the Fisher *r*-to-*z* normalization, transformed to the Talairach space, re-sampled to $2{\times}2{\times}2$ mm^3 isotropic voxel size, and spatially smoothed using isotropic Gaussian blur with FWHM = 5 mm. The single-subject fMRI-based PPI interaction maps were submitted to whole-brain group PPI analyses that employed the 3dttest++ AFNI program.

S1.6. EEG data analysis

Offline analysis of the EEG data was performed in BrainVision Analyzer 2.1 (Brain Products, GmbH). Removal of MR and cardioballistic (CB) artifacts was based on the average artifact subtraction (AAS) method (Allen et al., 1998, 2000) implemented in the Analyzer. The MR artifact template was defined using MRI slice markers recorded with the EEG data. After the MR artifact removal, the data were bandpass filtered between 0.5 and 80 Hz (48 dB/octave) and downsampled to 250 S/s sampling rate (4 ms interval). The fMRI slice selection frequency (17 Hz) and its harmonics were removed by band rejection filtering. The MR artifact removal was performed for the 27 EEG channels, the ECG channel, and the 4 reference artifact channels (re-purposed FC1, FC2, TP9, TP10). Removal of CB artifacts and follow-up analyses were conducted for the 27 EEG channels only. The CB artifact template was determined from the cardiac waveform recorded by the ECG channel, and the CB artifact to be subtracted was defined, for each EEG channel, by a moving average over 21 cardiac periods. Cardiac periods with strong rendom-motion artifacts were not included in the CB correction.

Following the MR and CB artifact removal, the EEG data from the five task runs (Fig. 1B) were concatenated to form a single dataset. The data were carefully examined, and intervals exhibiting significant motion or instrumental artifacts were marked manually as “bad intervals” and excluded from the analysis. The signals from the 4 reference artifact channels were taken into account to more reliably identify data intervals affected by random head motions and distinguish them from intervals exhibiting neuronal activity (e.g. theta). Channel FCz was kept as the EEG reference throughout the analysis.

An independent component analysis (ICA) was performed over the entire dataset with exclusion of the bad intervals. This approach ensured that independent components (ICs) corresponding to various artifacts were identified and removed in a consistent manner across all five runs. The Infomax ICA algorithm (Bell and Sejnowski, 1995), implemented in BrainVision Analyzer 2.1, was applied to the data from 27 EEG channels and yielded 27 ICs. Time courses, spectra, topographies, and kurtosis values of all the ICs were carefully analyzed to identify various artifacts, as well as EEG signals of neuronal origin. After all the ICs had been classified, an inverse ICA transform was applied to remove the identified artifacts from the EEG data. Because many artifacts had already been removed using the ICA, the data were examined again, and new bad intervals were defined to exclude remaining artifacts.

A time-frequency analysis was performed to compute EEG power for each channel as a function of time and frequency. The continuous wavelet transform with Morlet wavelets, implemented in BrainVision Analyzer 2.1, was applied to obtain EEG signal power in [0.5-30] Hz frequency range with 0.5 Hz frequency resolution and 4 ms temporal sampling. An EEG power as a function of time was then computed for each frequency band of interest.

S1.7. EEG-based PPI analyses

To investigate how temporal correlations between FAA (or FBA) and BOLD activity changed between experimental conditions, we performed PPI analyses adapted for EEG-fMRI (Zotev et al., 2014, 2016, 2018a). The analyses followed the standard fMRI-based PPI analysis approach (Friston et al., 1997; Gitelman et al., 2003), except that the initial deconvolution step, used to estimate an underlying neuronal activity from an fMRI time course, was skipped, and the actual EEG activity time course was employed. The EEG-based PPI analyses were conducted separately for the FAA and FBA time courses.

EEG-based PPI regressors for the FAA were defined as illustrated in Figure S3. The FAA values, computed with 4 ms temporal resolution for each experimental run, were averaged for 200-ms-long time bins. The resulting waveform was linearly detrended and orthogonalized with respect to the Happy Memories and Count stimulus waveforms (Fig. 1B) using the glmfit() MATLAB program. This procedure removed variations in mean FAA levels across the conditions to focus the analysis on temporal FAA variations around the means. The FAA time course was then converted to *z*-scores across each run. The HRF ('Cox special') was calculated with 200 ms sampling using the waver AFNI program. Convolution of the *z*(FAA) time course with the HRF by means of the conv() MATLAB program yielded a regressor, which we employed as the EEG-based PPI correlation regressor (Fig. S3A). An EEG-based PPI interaction regressor was defined for the Happy Memories vs Count condition contrast as follows. A [Happy−Count] contrast function was set to be equal +1 for the Happy Memories condition blocks, −1 for the Count condition blocks, and 0 for the Rest condition blocks (Fig. S3B). The *z*(FAA) time course was first multiplied by the [Happy−Count] contrast function, and then convolved with the HRF (Fig. S3C). The resulting waveform was used as the EEG-based PPI interaction regressor for the Happy Memories vs Count condition contrast. The two PPI regressors – correlation and interaction – were sub-sampled to the middle time points of fMRI volumes. Two additional PPI regressors were defined in the same way using the power-sum function instead of the FAA. Prior to its inclusion in the GLM model, the FAA-based PPI correlation regressor was linearly detrended and orthogonalized with respect to the corresponding power-sum-based PPI correlation regressor. Similarly, the FAA-based PPI interaction regressor was linearly detrended and orthogonalized with respect to the power-sum-based PPI interaction regressor. This procedure ensured that the two EEG-based PPI regressors specifically reflect temporal variations in the FAA rather than variations in the average power for the two channels. For the FBA, the PPI regressors were defined in a similar way starting with the FBA time course.

A single-subject EEG-based PPI analysis involved fitting a GLM model using the 3dDeconvolve AFNI program. The design matrix for each task run had the same structure as described above for the fMRI-based PPI analysis, except that the two EEG-based PPI regressors – interaction and correlation – were used instead of the fMRI-based PPI regressors. The resulting PPI interaction and correlation maps were subjected to the Fisher normalization, Talairach transform, re-sampling, and spatial smoothing as described above. Whole-brain group PPI analyses were conducted for the EEG-based PPI interaction maps using the 3dttest++ AFNI program. The analyses included two covariates: the participants' MADRS depression severity ratings and average individual values of the PPI interaction effect for a WM mask. The WM mask was defined for each participant as follows. The individual high-resolution anatomical brain image in the Talairach space (S1.4) was thresholded to select WM regions only, and the resulting mask was multiplied by the standard WM mask in the Talairach space (TT_wm+tlrc). The mask was then re-sampled to 2×2×2 mm^3 voxels, and subjected to erosion by one voxel to improve its separation from gray matter. The resulting individual WM mask in the Talairach space contained, on average, ~10000 voxels. The EEG-based PPI interaction values, averaged within this WM mask, were used as a covariate vector in the group analyses to better account for spurious PPI interaction effects. Such effects could be caused, e.g., by residual motion artifacts in the simultaneously acquired EEG and fMRI data.

S2.1. Verbal self-report performance ratings

Figure S4 exhibits average memory recall and happiness ratings for each group. The two ratings were reported verbally by each participant after each experimental run (except Rest). The EG vs CG group differences in the individual ratings averaged across the four nf runs trended toward significance after correction both for the memory recall ratings (EG vs CG, NF: $t(22)=2.29$, $p<0.032$, $q<0.064$, $d=0.99$) and the happiness ratings (EG vs CG, NF: $t(22)=1.90$, $p<0.071$, $q<0.071$, $d=0.82$). For the Transfer run, group differences were significant after correction for both ratings (Memory-recall, EG vs CG, TR: $t(22)=2.61$, $p<0.016$, $q<0.043$, $d=1.13$; Happiness, EG vs CG, TR: $t(22)=2.39$, $p<0.026$, $q<0.043$, $d=1.04$; corrected for the four tests).

S2.2. BOLD fMRI activity across the brain

Figure S5 exhibits whole-brain statistical maps of BOLD fMRI activity during the rtfMRI-EEG-nf training for the EG participants. The maps correspond to the Happy Memories vs Count condition contrast (H vs C). The individual-subject fMRI percent signal change maps were averaged for the four nf runs (PR, R1, R2, R3). The group mean was compared to zero using a one-sample *t*-test ($df=15$, two-tailed). The statistical results are summarized in Table S2. The maps in Fig. S5 are FDR corrected with $q<0.05$ threshold, and the data in Table S2 – with $q<0.01$ threshold. The results demonstrate significant positive BOLD activity contrast for the left amygdala region and many areas of the limbic system. They also reveal pronounced BOLD laterality for large parts of the middle frontal gyrus and superior frontal gyrus (Fig. S5, Table S2).

S2.3. Amygdala fMRI connectivity changes

Figure S6 shows whole-brain statistical maps for the EG vs CG group difference in the LA fMRI connectivity changes during the rtfMRI-EEG-nf training. The statistics are summarized in Table S3. The results reveal three loci in the rACC area, characterized by the most pronounced EG vs CG group differences: (−8, 34, 7) with $t=4.41$, (−9, 41, 5) with $t=4.04$, and (3, 35, 9) with $t=3.34$ (Table S3). These loci are pointed by green arrows in Fig. S6B. The EG vs CG group differences in fMRI connectivity changes between the LA and 10-mm-diameter spherical ROIs centered at these locations were significant with large effect sizes: $t(22)=3.31$, $p<0.003$, $d=1.43$ for the (−8, 34, 7) centered ROI; $t(22)=3.31$, $p<0.003$, $d=1.43$ for the (−9, 41, 5) centered ROI; and $t(22)=3.06$, $p<0.006$, $d=1.32$ for the (3, 35, 9) centered ROI. The average connectivity changes between the LA and the right rACC ROI centered at (3, 35, 9) showed significant negative correlation with the MADRS depression severity ratings for the EG ($r=-0.55$, $p<0.027$).

S2.4. Amygdala BOLD laterality interpretation

The amygdala BOLD laterality ('LA−RA') is a relevant metric for assessing target-specific effects of the rtfMRI-nf procedure aimed at upregulating the LA BOLD activity for the following reasons (Zotev et al., 2016). First, both the LA and RA are activated by happy emotion induction, as evidenced by substantial BOLD activations of the RA in our studies that used rtfMRI-nf of the LA activity (e.g. Zotev et al., 2011, 2016; Young et al., 2014). Second, emotional side effects that accompany performance of the difficult neurofeedback task (e.g. confusion, frustration, anxiety, etc.) conceivably involve activations of both the LA and RA. Third, due to the relative proximity of the LA and RA, their apparent BOLD activity levels may be affected by similar fMRI artifacts (e.g. signal losses due to magnetic susceptibility variations). Because only the LA BOLD activity (and not that of the RA) is explicitly upregulated using the rtfMRI-nf in our studies, the amygdala BOLD laterality is more sensitive to *target-specific* effects of the rtfMRI-nf procedure.

S2.5. fMRI correlates of the FBA modulation

Figure S8 shows whole-brain statistical maps for the FBA-based PPI interaction effect for the Happy Memories vs Count contrast for the EG. The group analysis was conducted in the same way as described for the FAA. Statistical results for the FBA-based PPI interaction effect are summarized in Table S4. The maps in Fig. S8 are voxel-wise FDR corrected at $q<0.07$ level, and the data in Table S4 – at $q<0.05$ level.

Similar to the results for the FAA (Fig. 11), the whole-brain maps of the FBA-based PPI interaction effect (Fig. S8) demonstrate that performance of the rtfMRI-EEG-nf task was associated with enhancement in temporal correlations between the FBA and BOLD activities of the large brain network. In particular, significant positive FBA-based PPI interaction effects are observed for the corresponding left and right DLPFC regions (MidFG, BA 9), with maxima at (−29, 35, 32) and (31, 41, 28), respectively (Fig. S8, Table S4). These maxima are located closer to the medial plane, than the similar maxima for the FAA-based PPI effect (Fig. 11, Table 2).

The results in Fig. S8 show the most pronounced FBA-based PPI interaction effects along the cortical midline and the cingulate gyrus, including the anterior and posterior cingulate (Fig. S8, Table S4). The statistical maximum is at (−19, 12, 42) in the left SFG (BA 8) and the effect extends down to the ACC (BA 32). Elevated high-beta activity in these areas, often with some lateralization to the right, is associated with anxiety (e.g. Zotev and Bodurka, 2020 and references therein). Significant FBA-based PPI interaction effects are also found for many regions involved in autobiographical memory retrieval, including the hippocampus, the extended areas of the parahippocampal gyrus, the anterior thalamus, the precuneus (BA 31), the posterior cingulate (BA 29), the lingual gyrus (involved in visual memory), and others (Fig. S8, Table S4). For the PMC areas (PrecG, BA 6), the FBA-based PPI interaction effects are less pronounced than the corresponding FAA-based effects.

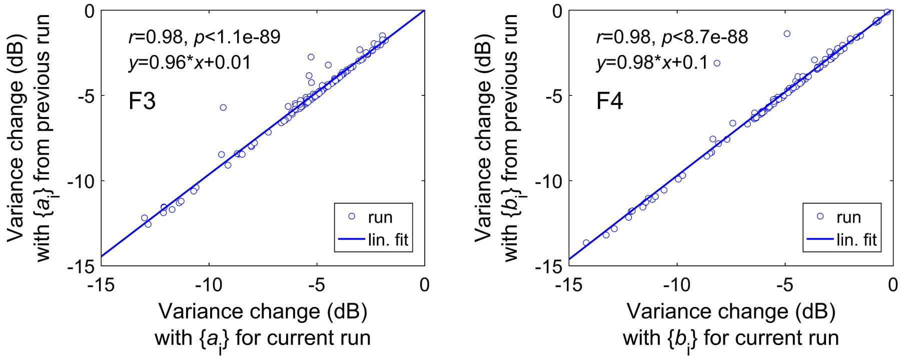

Figure S1. Effectiveness of the real-time EEG-fMRI artifact regression procedure with the regression coefficients $\{a_i\}$ and $\{b_i\}$ determined by fitting the data for the previous run (y-axis), compared to the effectiveness of a similar procedure with the optimum coefficients determined by fitting the data for the same (current) run (x-axis). Results for 120 experimental runs (24 participants, 5 task runs) are pooled together in each plot.

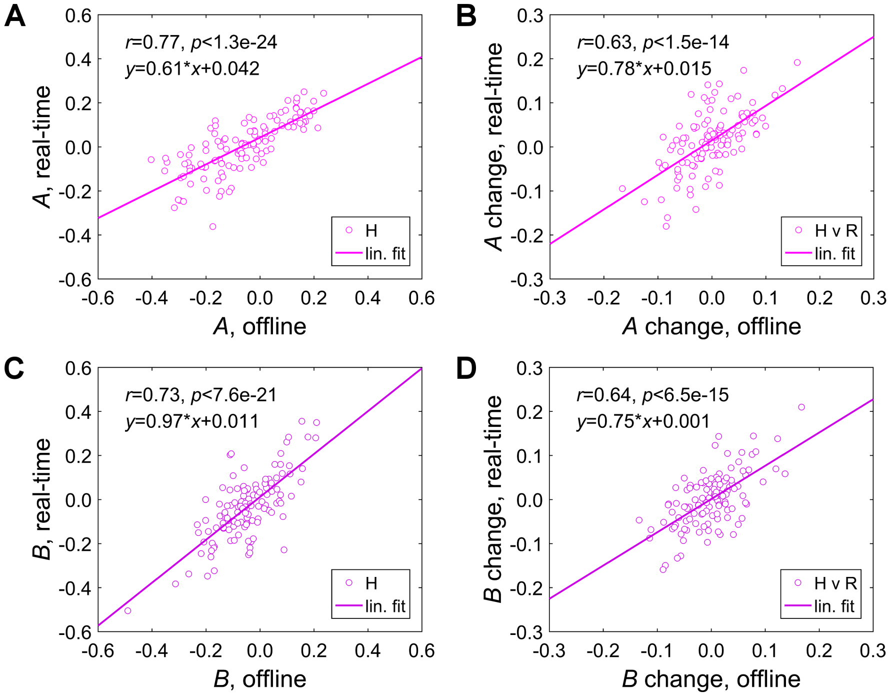

Figure S2. Comparison of relative frontal EEG asymmetry measures *A* (alpha band) and *B* (high-beta band), determined for the EEG data after the real-time processing and for the same data after the offline EEG data processing. Results for 120 experimental runs (24 participants, 5 task runs) are pooled together in each plot. A) Mean *A* values for the Happy Memories conditions in each run. B) Mean *A* changes between the Rest and Happy Memories conditions (H vs R) in each run. C) Mean *B* values for the Happy Memories conditions. D) Mean *B* changes between the Rest and Happy Memories conditions.

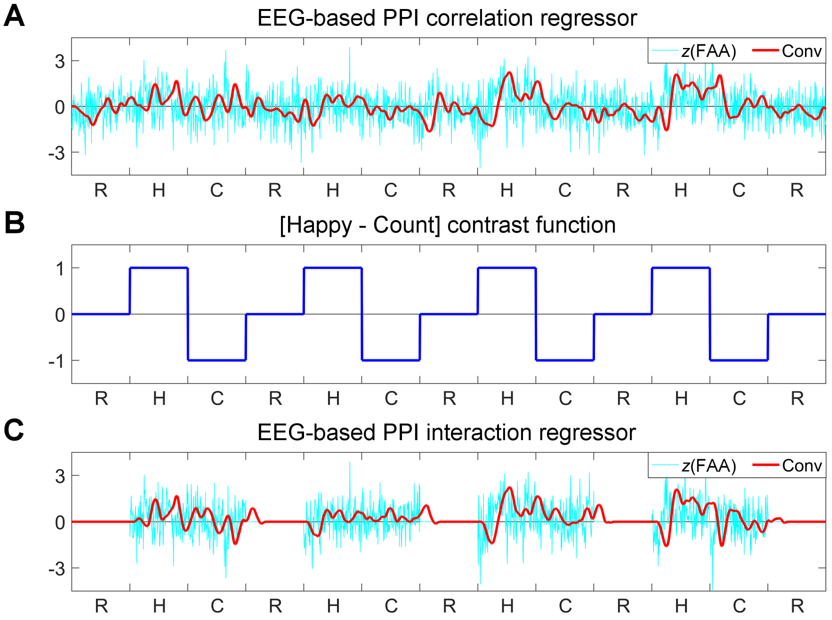

Figure S3. Definition of regressors for EEG-based psychophysiological interaction (PPI) analysis of fMRI data. A) Convolution of a time course of the FAA (converted to *z*-scores) with the HRF yields an EEG-based PPI correlation regressor. B) Contrast function for the Happy Memories (H) versus Count (C) conditions for one experimental run. C) Convolution of the FAA time course, multiplied by the contrast function, with the HRF yields an EEG-based PPI interaction regressor for the Happy Memories vs Count condition contrast.

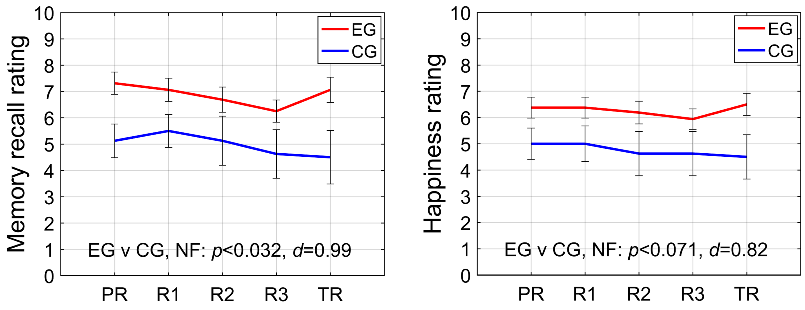

Figure S4. Average memory recall and happiness ratings reported by the participants after each experimental run. EG – experimental group, CG – control group. The error bars are standard errors of the mean (sem). The NF refers to group difference statistics (*p*-value from an independent-samples *t*-test and the corresponding effect size *d*) for the individual ratings averaged across the four nf runs (PR, R1, R2, R3).

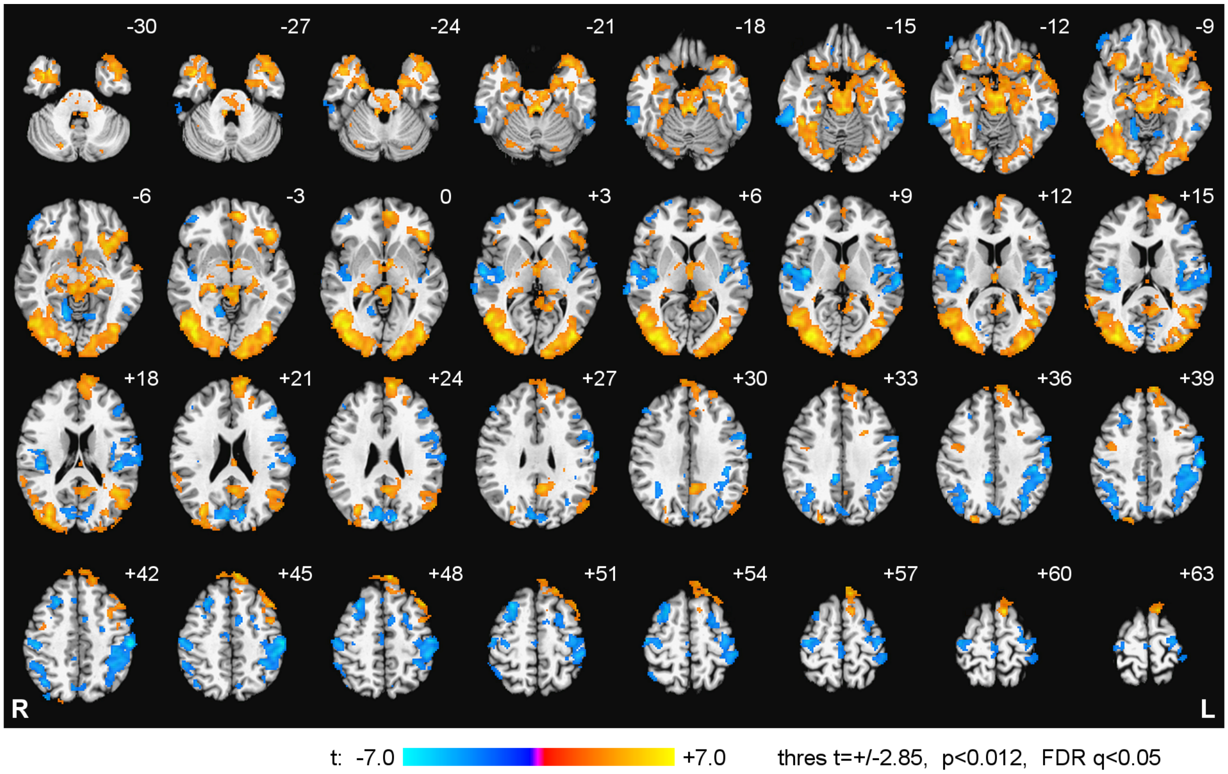

Figure S5. Statistical maps of BOLD fMRI activity, corresponding to the Happy Memories vs Count condition contrast, during the rtfMRI-EEG-nf training for the experimental group (EG). The individual fMRI activity results were averaged across the four nf runs (PR, R1, R2, R3). The maps are voxel-wise FDR corrected and projected onto the standard TT_N27 anatomical template in the Talairach space, with 3 mm separation between axial slices. The number adjacent to each slice indicates the *z* coordinate in mm. Following the radiological notation, the left hemisphere (L) is shown to the reader's right. The *t*-statistics maxima and minima and the corresponding locations are specified in Table S2.

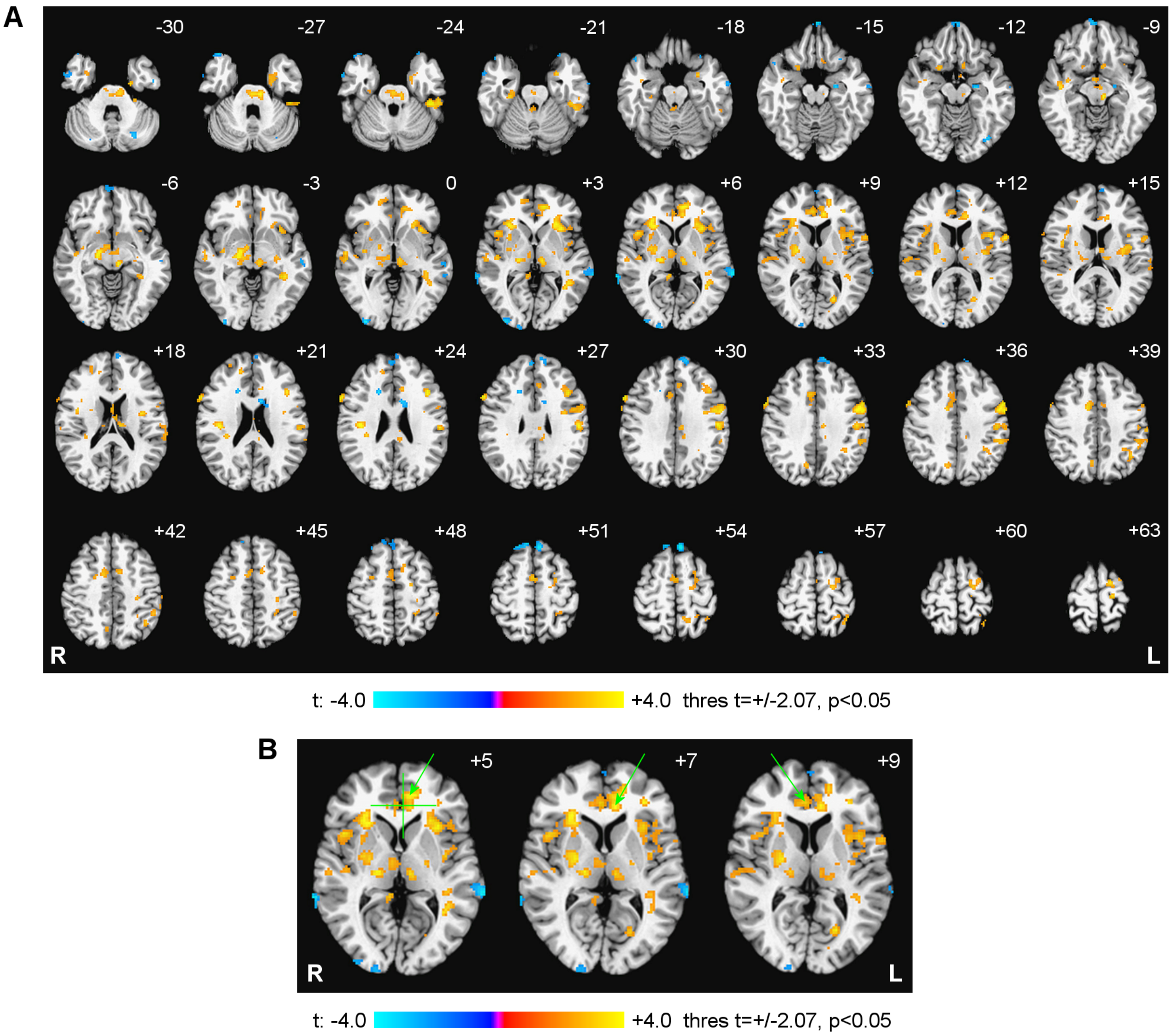

Figure S6. A) Statistical maps of the experimental vs control group difference (EG vs CG) in the left amygdala fMRI functional connectivity changes during the rtfMRI-EEG-nf training. The fMRI connectivity changes between the Rest and Happy Memories conditions (H vs R) were evaluated in the psychophysiological interaction (PPI) analysis, based on the LA time course. The individual PPI interaction results were averaged across the four nf runs (PR, R1, R2, R3). The maps are projected onto the standard TT_N27 anatomical template in the Talairach space. The number adjacent to each slice indicates the *z* coordinate in mm. Peak *t*-statistics values and the corresponding locations are specified in Table S3. B) Loci in the rACC area, which exhibited the largest EG vs CG group differences, are pointed by green arrows: (−8, 34, 7), (−9, 41, 5), and (3, 35, 9). The green crosshairs mark the center of the L rACC target ROI.

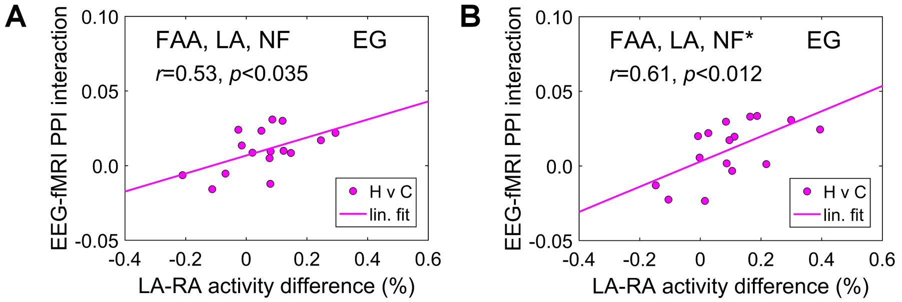

Figure S7. Correlations between average values of the amygdala BOLD laterality (‘LA−RA’) and the corresponding average values of the FAA-based PPI interaction effect for the LA ROI for the experimental group (EG). Both quantities correspond to the Happy Memories vs Count (H vs C) condition contrast. A) The individual results were averaged across the four nf runs (PR, R1, R2, R3). B) The individual results were averaged for three nf runs (out of four) with the most positive amygdala BOLD laterality values.

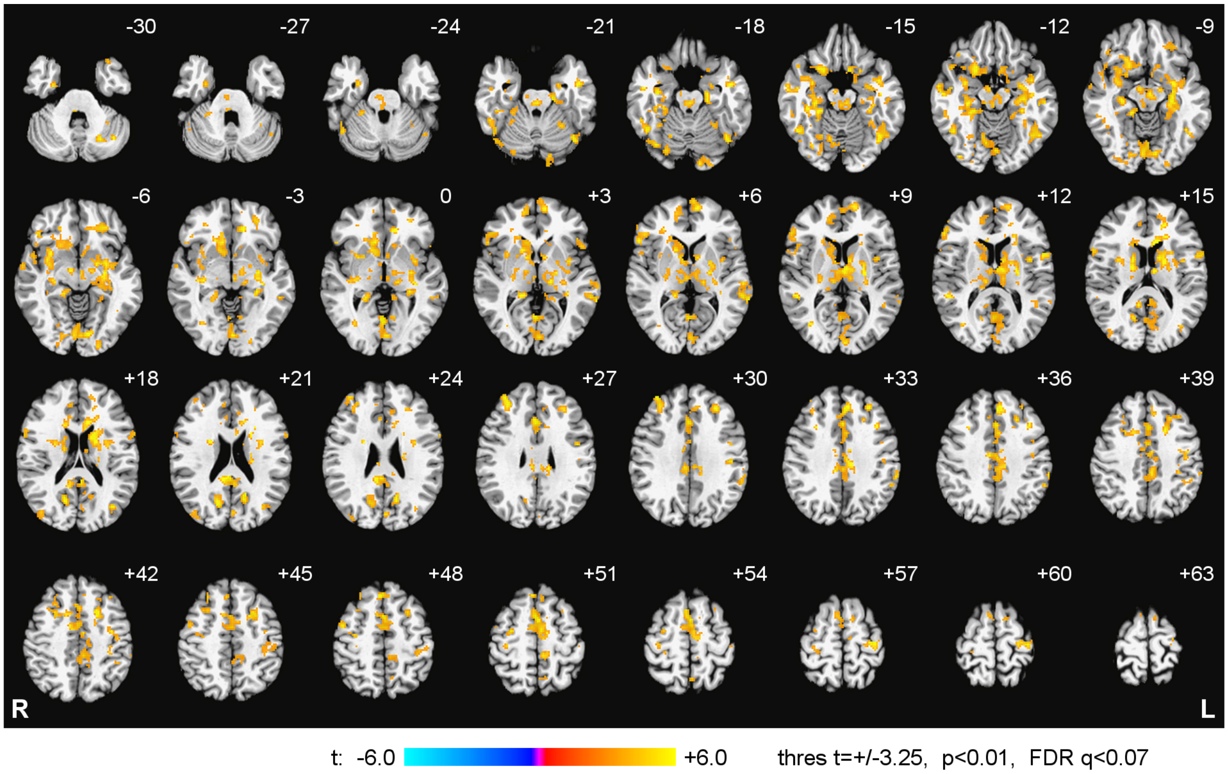

Figure S8. Enhancement in temporal correlation between frontal high-beta EEG asymmetry (FBA) and BOLD activity during the rtfMRI-EEG-nf training. Statistical maps of the FBA-based PPI interaction effect for the Happy Memories vs Count condition contrast (H vs C) are shown for the experimental group (EG). The maps are voxel-wise FDR corrected and projected onto the standard TT_N27 anatomical template, with 3 mm separation between axial slices. The number adjacent to each slice indicates the *z* coordinate in mm. The left hemisphere (L) is to the reader's right. Peak *t*-statistics values for the FBA-based PPI interaction effect and the corresponding locations are specified in Table S4.

Table S1. Psychological trait measures for the study participants. Psychological traits were assessed before the rtfMRI-EEG-nf session using the Hamilton Depression Rating Scale (HDRS), the Montgomery-Asberg Depression Rating Scale (MADRS), the Snaith-Hamilton Pleasure Scale (SHAPS), the Hamilton Anxiety Rating Scale (HARS), the State-Trait Anxiety Inventory (STAI), the Toronto Alexithymia Scale (TAS-20), and the Behavioral Inhibition System / Behavioral Activation System scales (BIS/BAS).

Measure	**Experimental group, mean (SD)**	**Control group, mean (SD)**	**Difference *t*-score [*p*]#**
Participants	16	8	
Age (years)	32 (11)	34 (7)	−0.67 [0.510]
HDRS	14.4 (7.0)	15.1 (4.9)	−0.25 [0.807]
MADRS	19.6 (10.7)	20.5 (5.7)	−0.23 [0.821]
SHAPS	27.1 (6.7)	31.5 (5.8)	−1.58 [0.129]
HARS	13.2 (7.5)	16.1 (6.4)	−0.95 [0.355]
STAI Trait anxiety	56.9 (9.9)	59.6 (9.6)	−0.65 [0.522]
TAS-20 Total alexithymia	53.5 (14.4)	61.8 (12.2)	−1.38 [0.180]
BAS Reward responsiveness	14.9 (3.3)	16.3 (2.4)	−0.99 [0.337]
BIS	22.4 (3.6)	24.1 (4.1)	−1.02 [0.319]

t(22), but *t*(19) for BIS/BAS; *p* – two-tailed, uncorrected

Table S2. BOLD fMRI activity, corresponding to the Happy Memories vs Count condition contrast, during the rtfMRI-EEG-nf training for the experimental group (EG).

Region	**Laterality**	***x*, *y*, *z* (mm)**	***t*-score**
Frontal lobe			
Inferior frontal gyrus (BA 47)	L	−33, 17, −18	8.26
Middle frontal gyrus (BA 8)	L	−40, 20, 47	7.21
Inferior frontal gyrus (BA 47)	L	−43, 29, −5	7.09
Superior frontal gyrus (BA 8)	L	−7, 49, 48	6.90
Superior frontal gyrus (BA 10)	L	−7, 60, 24	6.71
Inferior frontal gyrus (BA 13/47)	R	29, 14, −10	6.69
Superior frontal gyrus (BA 6)	L	−11, 13, 62	6.66
Superior frontal gyrus (BA 8)	R	27, 17, 49	−6.59
Superior frontal gyrus (BA 6)	L	−9, 31, 57	6.36
Temporal lobe			
Middle temporal gyrus (BA 37)	R	49, −59, 5	9.14
Superior temporal gyrus (BA 38)	R	39, 5, −28	7.90
Middle temporal gyrus (BA 37)	L	−42, −67, 11	6.65
Inferior temporal gyrus (BA 37)	L	−55, −45, −16	−5.66
Middle temporal gyrus (BA 20)	R	53, −35, −15	−5.35
Parietal lobe			
Postcentral gyrus (BA 2)	L	−55, −23, 44	−10.9
Precuneus (BA 7/19)	R	23, −81, 35	6.07
Inferior parietal lobule (BA 40)	L	−46, −33, 45	−5.29
Inferior parietal lobule (BA 39)	R	35, −63, 42	−5.24
Occipital lobe			
Middle occipital gyrus (BA 19/18)	R	39, −81, 2	9.70
Middle occipital gyrus (BA 19)	L	−39, −77, 2	8.26
Lingual gyrus (BA 17)	L	−19, −86, 1	6.69
Cuneus (BA 18)	L	−11, −79, 21	−5.64
Limbic lobe			
Parahippocampal gyrus (BA 36)	R	25, −31, −14	7.07
Anterior cingulate (BA 32)	L	−7, 49, −2	6.62
Amygdala / parahipp. gyrus	L	−29, −1, −14	6.55
Amygdala / uncus	L	−21, −3, −22	6.13
Cingulate gyrus (BA 31)	R	7, −39, 34	−6.10
Hippocampus / parahipp. gyrus	L	−28, −24, −9	6.00
Cingulate gyrus (BA 31)	L	−6, −49, 28	5.36
Sub-lobar			
Red nucleus	L	−7, −19, −10	8.43
Insula (BA 13)	R	37, −13, 12	−7.12
Insula (BA 13)	L	−39, −9, 6	−6.07
Thalamus, mediodorsal	R	2, −9, 2	5.76
Thalamus, mediodorsal	L	−1, −14, 8	5.53

FDR $q<0.01$ for $|t|>5.0$; BA – Brodmann areas; L – left; R – right; *x*, *y*, *z* – Talairach coordinates.

Table S3. Experimental vs control group difference in the left amygdala fMRI functional connectivity changes between the Rest and Happy Memories conditions (H vs R) during the rtfMRI-EEG-nf training.

Region	**Laterality**	***x*, *y*, *z* (mm)**	***t*-score**
Frontal lobe			
Inferior frontal gyrus (BA 9)	R	57, 13, 32	5.73
Middle frontal gyrus (BA 9)	L	−53, 8, 36	4.63
Superior frontal gyrus (BA 6)	L	−7, 33, 54	−4.56
Precentral gyrus (BA 6)	L	−51, 1, 33	4.49
Middle frontal gyrus (BA 9/46)	L	−39, 19, 24	4.42
Superior frontal gyrus (BA 6)	L	−15, −7, 64	3.68
Inferior frontal gyrus (BA 44)	L	−55, 5, 14	3.67
Medial frontal gyrus (BA 11)	L	−3, 61, −14	−3.64
Superior frontal gyrus (BA 6)	R	9, 37, 52	−3.47
Temporal lobe			
Fusiform gyrus (BA 20)	L	−43, −31, −24	5.22
Superior temporal gyrus (BA 22)	L	−67, −35, 6	−3.82
Superior temporal gyrus (BA 21)	R	55, −13, 0	3.31
Parietal lobe			
Postcentral gyrus (BA 2)	L	−51, −19, 28	4.37
Inferior parietal lobule (BA 40)	L	−47, −37, 38	3.28
Occipital lobe			
Middle occipital gyrus (BA 18)	R	31, −91, 2	−4.01
Limbic lobe			
Anterior cingulate (BA 24)	L	−8, 34, 7	4.41
Parahippocampal gyrus (BA 37)	L	−33, −39, −4	4.36
Anterior cingulate (BA 32)	L	−9, 41, 5	4.04
Cingulate gyrus (BA 24)	R	11, 1, 38	4.01
Uncus (BA 36)	L	−21, −9, −30	3.62
Anterior cingulate (BA 24)	R	3, 35, 9	3.34
Sub-lobar			
Subthalamic nucleus	R	15, −13, −4	7.39
Red nucleus	L	−7, −25, −6	4.44
Insula (BA 13)	R	29, 21, 4	4.29
Insula (BA 13/47)	L	−31, 15, 4	4.15
Thalamus, ventroposterolateral	R	17, −19, 6	3.95
Claustrum	L	−31, −11, 14	3.91
Putamen	R	23, −9, 8	3.79

p<0.05, uncorr. BA – Brodmann areas; L – left; R – right; *x*, *y*, *z* – Talairach coordinates

Table S4. Psychophysiological interaction effect, based on the time course of frontal high-beta EEG asymmetry (FBA), for the Happy vs Count contrast for the experimental group (EG).

Region	**Laterality**	***x*, *y*, *z* (mm)**	***t*-score**
Frontal lobe			
Superior frontal gyrus (BA 8/32)	L	−19, 12, 42	11.8
Medial frontal gyrus (BA 6)	L	−5, 35, 36	10.2
Superior frontal gyrus (BA 8)	R	3, 29, 50	9.58
Inferior frontal gyrus (BA 44)	L	−51, 6, 13	8.75
Medial frontal gyrus (BA 6)	L	−1, 3, 52	7.93
Middle frontal gyrus (BA 9)	L	−29, 35, 32	7.79
Precentral gyrus (BA 4)	L	−29, −21, 58	7.52
Middle frontal gyrus (BA 9)	R	31, 41, 28	7.30
Precentral gyrus (BA 6)	R	27, −9, 52	6.23
Medial frontal gyrus (BA 10)	L	−9, 55, 6	6.12
Temporal lobe			
Middle temporal gyrus (BA 39)	L	−37, −69, 18	7.91
Superior temporal gyrus (BA 41)	R	49, −37, 10	7.58
Middle temporal gyrus (BA 20)	L	−45, −5, −20	7.42
Superior temporal gyrus (BA 22)	L	−63, −41, 6	6.88
Middle temporal gyrus (BA 21)	R	59, −7, −12	6.37
Parietal lobe			
Precuneus (BA 31)	L	−13, −59, 24	9.79
Precuneus (BA 31)	R	15, −63, 20	8.16
Occipital lobe			
Lingual gyrus (BA 18)	L	−9, −79, −6	7.20
Limbic lobe			
Anterior cingulate (BA 33)	L	−9, 19, 16	10.3
Posterior cingulate (BA 29)	R	3, −39, 20	9.53
Anterior cingulate (BA 32)	L	−13, 33, −2	9.36
Parahippocampal gyrus (BA 30)	R	17, −37, 4	8.40
Parahippocampal gyrus (BA 36)	R	24, −33, −14	8.19
Cingulate gyrus (BA 32)	L	−1, 21, 28	7.94
Subcallosal gyrus (BA 47)	R	20, 11, −12	7.65
Cingulate gyrus (BA 31)	L	−10, −25, 34	7.61
Hippocampus / parahipp. gyrus	L	−27, −23, −10	7.41
Hippocampus / parahipp. gyrus	L	−27, −33, −3	7.29
Amygdala / parahipp. gyrus	L	−28, −5, −10	6.94
Parahippocampal gyrus (BA 28)	L	−19, −23, −18	6.58
Sub-lobar			
Thalamus, ventral anterior	R	15, −9, 15	9.12
Declive	R	33, −69, −17	9.12
Putamen	L	−23, −13, 8	9.10
Culmen of vermis	R	1, −61, 2	8.64
Claustrum	R	29, 7, −6	8.14

Caudate body	L	−16, 5, 18	7.87
Declive	L	−39, −61, −20	7.52
Thalamus, anterior	L	−7, −11, 15	7.50
Thalamus, mediodorsal	L	−3, −10, 10	7.21
Insula (BA 13)	L	−39, −1, 14	6.86

FDR $q<0.05$ for $|t|>6.0$; BA – Brodmann areas; L – left; R – right; x, y, z – Talairach coordinates.